Adsorption sites of individual metal atoms on ultrathin MgO(100) films

Edgar Fernandes,[1] Fabio Donati,[1] François Patthey,[1] Srdjan Stavrić,[2] Željko Šljivančanin,[2,3] and Harald Brune[1,*]

[1]*Institute of Physics, Ecole Polytechnique Fédérale de Lausanne, Station 3, CH-1015 Lausanne, Switzerland*
[2]*Vinča Institute of Nuclear Sciences (020), University of Belgrade, P.O.Box 522, 11001 Belgrade, Serbia*
[3]*The Science Program, Texas A&M University at Qatar, Doha, Qatar*

We use Ca doping during growth of one- and two-monolayer-thick MgO films on Ag(100) to identify the adsorption sites of individual adatoms with scanning tunneling microscopy. For this we combine atomic resolution images of the bare MgO layer with images of the adsorbates and the substitutional Ca atoms taken at larger tip-sample distance. For Ho atoms, the adsorption sites depend on MgO thickness. On the monolayer, they are distributed on the O and bridge sites according to the abundance of those sites, 1/3 and 2/3, respectively. On the MgO bilayer, Ho atoms populate almost exclusively the O site. A third species adsorbed on Mg is predicted by density functional theory and can be created by atomic manipulation. Au atoms adsorb on the bridge sites for both MgO thicknesses, while Co and Fe atoms prefer the O sites, again for both thicknesses.

I. INTRODUCTION

Single atoms on ultrathin insulating layers grown on metal surfaces have spectacular magnetic properties [1–3], in particular very long spin coherence [4] and even longer spin-relaxation times [5–7], making single-adatom qubits and memories feasible. Moreover, they exhibit multiple stable charge states [8–10]; when adsorbed in the vicinity of defects, they may catalyze chemical reactions [11]. Additionally, on surfaces of bulk oxides they are astonishingly stable [12] and are currently considered as single-atom catalysts [13–15]. These remarkable properties emerge from the interaction of the atom with the surface depending critically on the adsorption site. Knowing this site is therefore mandatory to understand the thermal stability, catalytic properties, charge state, and, finally, the symmetry of the crystal field that determines the lifetime of magnetic quantum states [16].

Field ion microscopy reveals the adsorption site but is limited to strongly bound species on metal surfaces [17]. Scanning tunneling microscopy (STM) and atomic force microscopy (AFM) are more versatile and are now widely employed to determine the adsorption sites of adatoms. However, all examples in the literature are limited to single-element surfaces [18–21]. On the surfaces of ionic crystals or thin films, such as MgO or NaCl, one often ignores which of the two sublattices gives rise to the atomic STM and AFM contrast. Density functional theory (DFT) calculations report contradicting results about the STM contrast on MgO/Ag(100) [22–24], while AFM contrast of NaCl was interpreted based on molecular markers for which the adsorption geometry was obtained from DFT [25,26]. Specific to STM, the tunnel parameters required for atomic resolution on insulating layers imply very small tip-sample distances. Under these conditions, adsorbed atoms are frequently displaced or even desorbed, which further complicates the determination of their adsorption site. For example, light adsorbates such as H can get displaced by tip-sample interactions even under moderate tunnel conditions, yielding fictitious adsorption sites [27]. As an alternative approach, electron paramagnetic resonance

(EPR) was used to indirectly identify the adsorption site of Au on thick MgO layers [28]. However, for the same atoms on three monolayers of MgO on Ag(100), the adsorption site is still debated [29–31]. These issues are general for any single atom on the surfaces of ionic crystals or thin films and call for a direct and reliable experimental method.

Here we introduce dilute Ca doping to mark the Mg sublattice in STM images of one- and two-monolayer-thick MgO films grown on Ag(100). To determine the orientation and size of the atomic MgO lattice, we record atomic resolution images on adsorbate-free areas. This lattice is overlaid onto STM images of the Ca dopants and adsorbates taken at larger tip-sample distance. On this grid all Ca atoms are on identical sites, demonstrating the reliability of our method to mark the Mg positions. A comparison of the adsorbates' positions with this MgO grid unequivocally identifies the adsorption sites of Ho, Au, Co, and Fe adatoms as a function of MgO thickness. These four elements are motivated by Ho being the first single-atom magnet [5], the adsorption sites of Au being debated [29–31], Co having the highest possible magnetocrystalline anisotropy for a $3d$ element [3], and, finally, Fe on MgO being the first system where electron spin resonance (ESR) with the STM was demonstrated [4] and where spin-coherence times were measured on a single atom. DFT calculations reveal the charge transfer and binding energy of the adsorbates on mono- and bilayer MgO/Ag(100), as well as on the (100) surface of bulk MgO.

We start by giving details of the experiment and of the DFT calculations in Sec. II. The results and discussion section is divided into five parts. Section III A focuses on the characterization of the pristine and Ca-doped MgO thin films. Sections III B and III C describe the experimental determination of the adsorption sites of Ho, as well as STM atomic manipulation experiment with these atoms. Sections III D and III E present results on the adsorption site of Co, Fe, and Au. Section IV concludes the paper.

II. TECHNICAL DETAILS

A. Experiment

The Ag(100) surface was prepared in ultrahigh vacuum by repeated cycles of Ar^+ sputtering (800 eV, 10 μA/cm^2) and

*Corresponding author: harald.brune@epfl.ch

subsequent annealing to 770 K. MgO thin films were grown by evaporating Mg from a Knudsen cell under a partial pressure of oxygen of 1×10^{-6} mbar and with the sample kept at 770 K, as described in Ref. [32]. These conditions yield an MgO growth rate of about 0.1 monolayer per minute. We define one monolayer (ML) as one MgO(100) unit cell per Ag(100) substrate atom. Calcium-doped MgO films were prepared by coevaporating Ca and Mg under the conditions described above and with a Ca flux significantly lower than the Mg flux, adjusted to obtain the desired dopant concentration. Ho, Co, Fe, and Au atoms were evaporated from *e*-beam evaporators onto the sample in the STM at $T_{\text{dep}} \approx 10$ K and with a base pressure below 1×10^{-10} mbar. STM measurements were performed with a home-built STM at $T_{\text{STM}} = 4.7$ K using W or PtIr tips [33]. Differential conductance (dI/dV) spectra were acquired with a lock-in amplifier using a bias modulation at 1397 Hz and working with the feedback loop closed to minimize the tip-surface interaction at large biases.

B. Density functional theory calculations

The DFT calculations for Ho adatoms on MgO(100)/Ag(100) were carried out using the WIEN2K computer code [34], with the same computational setup as the one described in Ref. [5], i.e., using the generalized gradient approximation (GGA) and on-site Coulomb interactions. DFT calculations of the Co and Au adatoms on thin MgO(100) films on Ag(100) were performed with the GPAW code [35], based on the real-space grid implementation of the projector augmented wave (PAW) method [36,37]. Exchange-correlation effects were described employing the Perdew-Burke-Ernzerhof functional (PBE) [38]. For Co, the calculations were performed within the GGA+U approach [39,40], which combines the standard PBE exchange-correlation functional with on-site Coulomb interaction, using a U value of 2 eV. The MgO(100)/Ag(100) surface was modeled with a 3×3 unit cell containing nine Mg and nine O atoms per MgO(100) layer, placed on a three-layer metal slab with nine Ag atoms per fcc(100) layer. In all calculations we used theoretically optimized Ag lattice constants of 4.14 Å, grid spacing of 0.15 Å, two-dimensional periodic boundary conditions parallel to the (100) surfaces, and 16 Monkhorst-Pack **k** points for sampling the Brillouin zone [41]. Open boundary conditions are applied perpendicular to the surface with 7 Å of vacuum separating the oxide/metal slabs from the cell boundaries. To increase numerical stability of the calculations, the electronic states were occupied according to the Fermi-Dirac distribution with a broadening of 0.1 eV. Atomic positions were relaxed using the Broyden-Fletcher-Goldfarb-Shanno algorithm [42].

III. RESULTS AND DISCUSSION

A. STM characterization of pristine and Ca-doped MgO thin films

Figure 1(a) shows an STM image of the MgO/Ag(100) surface with the bare substrate coexisting with MgO layers of two thicknesses. Since their apparent heights are strongly bias dependent and sometimes inverted with respect to the expectation from morphology [43], we use the energies of
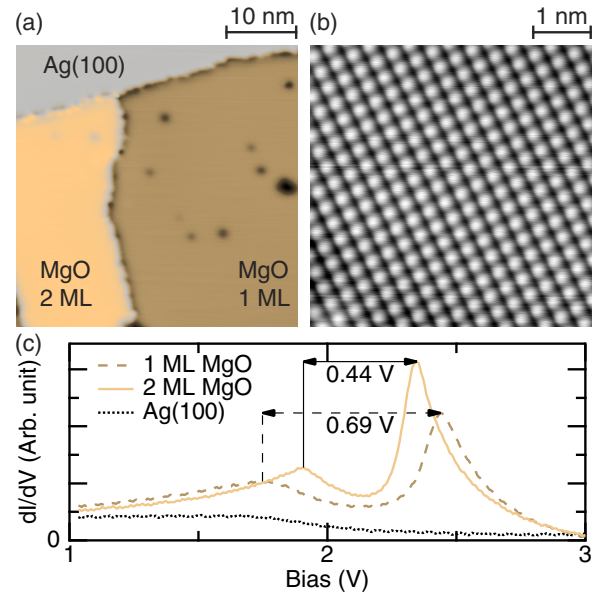

FIG. 1. (a) STM image of Ag(100) partially covered by MgO ($V_t = 0.12$ V, $I_t = 100$ pA). Dark spots are attributed to point defects in the oxide at the interface. (b) Atomically resolved image of 2-ML MgO ($V_t = -10$ mV, $I_t = 10$ nA). (c) Field emission resonance spectra recorded above 1- and 2-ML MgO as well as clean Ag(100) ($V_t = 0.12$ V, $I_t = 100$ pA, peak-to-peak modulation amplitude $V_{\text{mod}} = 10$ mV).

field emission resonances to determine the MgO thickness [44]. The dI/dV spectra in Fig. 1(c) exhibit two resonances with distinct energy separations of 0.69 V and 0.44 V; the first is characteristic of the MgO monolayer, and the second of the bilayer [44]. Note that a very recent paper [6] proposed an MgO thickness calibration that differs by one layer from the one used in the current literature and also in the present study. Our method to determine the adsorption sites is independent of the MgO thickness calibration used, only in the comparison of the experiment with DFT the MgO thickness does play a role.

The atomically resolved STM image of 2-ML MgO of Fig. 1(b) shows a square lattice of protrusions representing one ionic sublattice [29,44]. The period of 2.90 ± 0.03 Å agrees very well with the Ag(100) nearest-neighbor distance of 2.89 Å. In addition, the STM image shows no superstructure, such as moiré patterns or dislocations. Both observations provide direct evidence of the MgO(100) film being uniformly and compressively strained by 3% to form a pseudomorphic (1×1) structure on Ag(100). This confirms early diffraction studies [45] that revealed that this lateral compression leads to a vertical expansion of the unit cell by 3.6% [46]. Whether the protrusions in this image represent the Mg or the O species has been a matter of debate in theory [22–24]. Our Ca-doping method introduced hereafter determines it unequivocally for the respective STM tip and tunnel parameters.

Figure 2 shows an overview image of 1- and 2-ML Ca-doped MgO. For the employed tunnel parameters, Ca atoms are imaged as small protrusions with apparent heights of 73 ± 2 pm and 61 ± 2 pm, respectively, on 1- and 2-ML MgO. The extremely narrow apparent height distribution found for
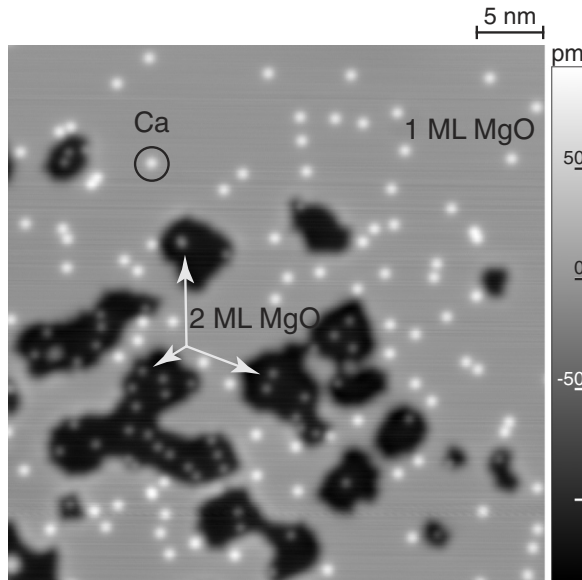
FIG. 2. STM image of one and two monolayers of MgO with the substitutional Ca atoms appearing as protrusions ($V_t = -515$ mV, $I_t = 100$ pA). Note that the apparent height of the MgO layers is inverted with respect to their thickness.

each of the two MgO thicknesses indicates that all Ca atoms are on identical lattice sites (uncertainties are calculated from the standard deviation of the object's apparent height, i.e., 88 and 50 objects, respectively, on 1- and 2-ML MgO). In addition, the very similar apparent heights observed on 1- and 2-ML MgO suggest that all Ca atoms are localized in the topmost MgO layer. Ca atoms buried in the second layer would appear with a different apparent height and would be located on the other lattice site. Therefore, Ca protrusions always mark the Mg lattice positions of the topmost layer irrespective of the local MgO thickness. Our conclusion of Ca surface segregation is supported by the literature [47–49]. Upon annealing of Ca-rich MgO crystals, Mg atoms at the surface are replaced with Ca. For our employed Ca doping of the order of 0.5% practically all the Ca atoms are sufficiently far from each other to appear as individual and identical protrusions (see Figs. 2 and 4).

B. Adsorption sites determination of Ho adatoms on thin MgO films

Figures 3(a) and 3(b) show 5×10^{-3} ML of Ho deposited at 10 K on 1- and 2-ML of MgO/Ag(100). While two species with characteristic apparent heights coexist on 1-ML MgO, on 2-ML the species with smaller apparent height (Ho^A) occurs almost exclusively.

Figure 4 shows a single MgO layer with substitutional Ca atoms, as well as both adsorbed Ho species. Calcium atoms appear as faint spots with an apparent height of 67 ± 12 pm for this tunneling set-point. Note that the higher uncertainty stems from the standard deviation obtained from the five Ca protrusions. The tunneling conditions yielding atomic resolution on MgO move the Ho atoms, and therefore, we imaged a bare MgO spot of the same sample with atomic resolution and extracted the orientation and lattice constant of the MgO lattice from it. This lattice was then overlaid onto Fig. 4, and one of its Mg atoms was aligned with one of
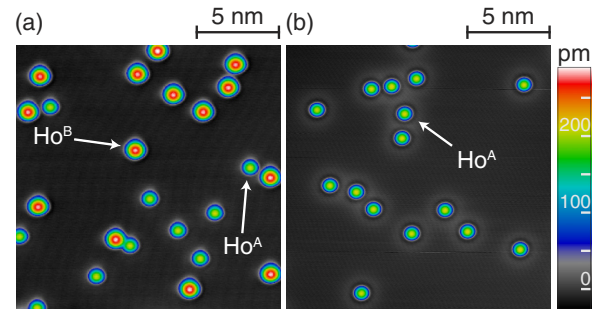

FIG. 3. STM images of (a) 1-ML and (b) 2-ML undoped MgO after the adsorption of 5×10^{-3} ML of Ho. Two species, Ho^A and Ho^B, are discerned by their apparent heights of 220 ± 4 pm and 295 ± 3 pm, respectively ($T_{dep} \approx 10$ K, $V_t = -20$ mV, $I_t = 20$ pA).

the substitutional Ca atoms. All other Ca species fall exactly onto Mg sites, illustrating the precision of the alignment. This technique has been applied on images up to 20×20 nm^2 containing up to 12 Ca atoms (not shown here) with the same reliability. Comparing the Ho positions with the overlaid MgO lattice for the shown image and for many additional ones, we infer that Ho^A adsorbs on O while Ho^B is on a bridge site. Thus, the preferred adsorption site on two MgO layers is on top of oxygen. In agreement, our DFT calculations identify this site for 2-ML MgO/Ag(100) as the most stable one (see Table I). They also show that this site is favored for MgO(100) bulk. Therefore, from 2-ML MgO on, the ensemble of Ho atoms is dominated by a single species. This facilitates the interpretation of ensemble measurements, such as x-ray magnetic circular dichroism [5].

The very different abundances of both Ho species on 1- and 2-ML MgO can be traced back to MgO thickness-dependent dissipation of the adsorption energy. On 1-ML
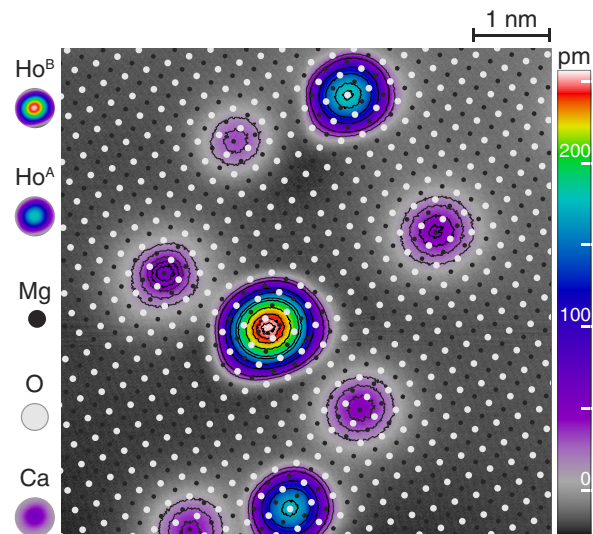

FIG. 4. STM image of 1-ML MgO grown with 5×10^{-3} ML Ca doping and the same number density of Ho atoms adsorbed onto it. The orientation and spacing of the overlaid MgO lattice were determined from an atomically resolved image recorded on a bare MgO spot of the same sample. This lattice was then translated to bring one of its Mg atoms in coincidence with one of the Ca species ($V_t = -20$ mV, $I_t = 20$ pA).

TABLE I. DFT binding-energy differences ΔE (eV) and charge transfers Δq (e) for individual Ho, Au, and Co atoms on O, bridge (br), and Mg sites on 1- and 2-ML-thick MgO/Ag(100) and on the (100) surface of MgO bulk. The site with the highest binding energy is taken as the reference; positive values signify a decrease in binding energy.

Atom	Site	1-ML MgO/Ag		2-ML MgO/Ag		MgO(100)	
		ΔE	Δq	ΔE	Δq	ΔE	Δq
Ho	O	0.90	0.26	0.00	0.12	0.00	−0.06
	br	0.33	0.56	0.19	0.71	0.61	−0.42
	Mg	0.00	1.20	0.21	1.21		
Au	O	0.04	−0.77	0.18	−0.80	0.00	−0.28
	br	0.00	−0.77	0.00	−0.83	0.15	−0.31
	Mg	0.19	−0.73	0.18	−0.79	0.35	−0.26
Co	O	0.00	0.14	0.00	0.01	0.00	−0.13
	br	0.09	0.52	0.12	0.45	0.29	−0.09
	Mg	0.52	0.92				

MgO, the abundance of both species (Ho^A: $35.8\% \pm 1.6\%$, Ho^B: $64.2\% \pm 1.6\%$) reflects that of their adsorption sites since there are two times more bridge than O sites. This is compatible to statistical growth, where the atoms come to rest at their site of impact, irrespective of its adsorption energy. The clear preference of the O site for 2-ML MgO (Ho^A: $91.5\% \pm 1.7\%$, Ho^B: $8.5\% \pm 1.7\%$) implies adatom motion. Thermal mobility can be ruled out since both species are immobile for hours up to 50 K. Therefore, the Ho atoms exhibit transient mobility, at least from the bridge toward the adjacent O site [50]. The fact that this occurs more readily on 2-ML MgO than on 1-ML MgO is related to the dissipation of the adsorption energy via electron-hole pair excitation in the substrate [51,52], which is more efficient for atoms adsorbing on thinner MgO layers.

C. STM manipulation of Ho adsorption sites

On 1-ML MgO/Ag(100), the DFT calculations identify the Mg site as the most favorable one for Ho atoms. Although Ho atoms do not spontaneously reach this site after deposition, we can populate it by atomic manipulation. For this we apply voltage ramps with the STM tip placed above the Ho atoms. To prevent major modifications of the probed area by high electric fields, the voltage is ramped while keeping the feedback loop closed; that is, the tunneling current stays constant while the tip retracts smoothly. Abrupt changes in the vertical position of the tip detected during the ramp evince a modification or a displacement of the probed atom [8]. Figures 5(a)–5(c) illustrate the result of this process on a few selected Ho atoms on 1-ML MgO. Ramping the bias up to -1 V on the Ho^A atoms [Fig. 5(a)] switches them to Ho^B. As a result, in Fig. 5(b) all the atoms have the same apparent height and are adsorbed on the bridge site. We note that this operation is reversible; that is, positive-bias ramping up to $+1$ V on top of a Ho^B transforms it back into Ho^A. Conversely, further ramping with negative biases up to -1.2 V on top of Ho^B atoms irreversibly switches them to a new species, Ho^C [see Fig. 5(c)]. With an apparent height of 141 ± 3 pm, this species appears much smaller than Ho^A or Ho^B. Similar atomic manipulations yield an equivalent
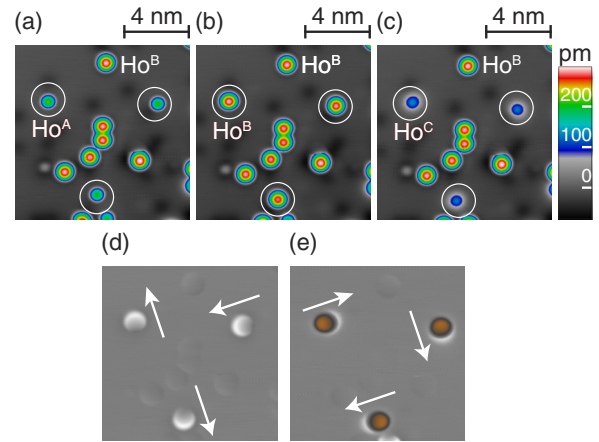

FIG. 5. STM images of Ho atoms on 1-ML MgO. Atoms indicated with circles are successively transformed from (a) Ho^A to (b) Ho^B and finally to (c) Ho^C by applying negative voltage ramps; see text for details [in (a)–(c), $V_t = -100$ mV, $I_t = 20$ pA]. (d) Subtraction of image (a) from (b) using the unchanged atoms for precise alignment. (e) Subtraction of (b) from (c). White (brown) indicates levels above (below) the zero plane. Arrows indicate the directions of the atomic displacements.

sequence of adsorption sites also on two MgO layers. Using the unchanged atoms as reference, we identify the possible displacement of the switched adatoms by subtracting subsequent images. Figure 5(d), obtained by subtracting Fig. 5(a) from Fig. 5(b), shows asymmetric spots at the positions of the three circled atoms. The white arrows point in the direction of the displacement and indicate that the switched atoms have moved along two perpendicular directions, which correspond to the two possibilities of hopping from an O to a bridge site. By subtracting Fig. 5(b) from Fig. 5(c), we observe that the switched atoms have been displaced perpendicular to their
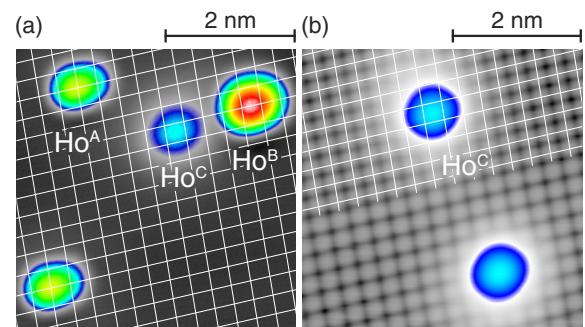

FIG. 6. (a) STM image of all three Ho species on 1-ML MgO ($V_t = -20$ mV, $I_t = 20$ pA). Ho^C has an apparent height of 141 ± 3 pm and is adsorbed on Mg. The lattice is again inferred from an atomically resolved image of the bare MgO surface and marks the O atoms of the MgO. (b) Atomically resolved image of two Ho^C atoms on 2-ML MgO. The lattice marks the O atoms that appear as protrusions ($V_t = -20$ mV, $I_t = 5$ nA). Note that (b) was recorded using the same tunneling parameters all along the image scan. The grid overlays the atomic protrusions, located at O lattice positions. Only half of the grid is shown to better distinguish the atomic protrusions in the lower part.
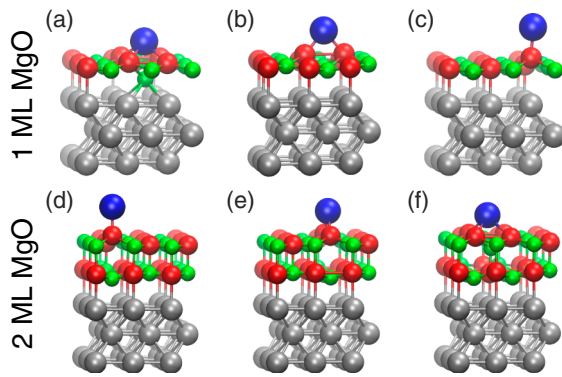
FIG. 7. DFT adsorption geometries of a Ho adatom on (a)–(c) one and (d)–(f) two MgO monolayers in order of decreasing binding energy from left to right. Color legend: red, O; green, Mg; gray, Ag; blue, Ho.

previous direction, i.e., from a bridge to an Mg site [see Fig. 5(e)].

Ho^C adatoms are remarkably stable. Voltage ramps up to ± 10 V have no effect on them, while Ho^A and Ho^B are transformed or desorbed under these conditions. Figure 6(a) shows the adsorption site of Ho^C to be on top of Mg. The grid marks the O sites and was determined with the same method as the one used for Fig. 4.

As shown by our DFT calculations for 1-ML MgO, this extraordinary stability results from a strong relaxation of the surrounding O neighbors and of the underlying Mg atom, making this binding site fourfold O coordinated [see Fig. 7(a)]. In agreement with experiment, this site has the highest binding energy, followed by the bridge and O sites, whose atomic geometries are shown in Figs. 7(b) and 7(c), respectively. See Table I for the differences in binding energy and charge state of the atoms in the respective sites.

On 2-ML MgO, adsorption on top of Mg is calculated to be less favorable due to the presence of the subsurface MgO

layer preventing large relaxation of the surface lattice [see Fig. 7(f)]. Nevertheless, experiment still finds this site to be the most stable one, although it is reachable only after atomic manipulation. Note also that the order of the charge states is in agreement with the atomic manipulation from O via bridge to Mg sites, requiring increasingly negative voltages. As also observed for Au and Ag on NaCl(100) [8–10], this indicates that the atoms become more and more positively charged along the transformation sequence.

The stability of the Ho^C species enables imaging it under tunnel conditions that yield atomic resolution on MgO. These conditions displace or desorb Ho atoms adsorbed on the other two sites. The lattice overlaid onto Fig. 6(b) marks the O atoms that appear as protrusions. According to our experience, this contrast is by far the most common one in low-bias images of the MgO surface. Only in very rare cases of tip chemistry and tunnel parameters are the Mg atoms imaged as protrusions. This clarifies the controversial DFT results on the STM contrast of MgO/Ag(100) [22–24].

D. Adsorption site of Co and Fe on MgO

Our method of Ca doping can be applied to determine the adsorption site of any adatom on MgO. Once the site of one species is determined, one can use that species as a marker to identify the sites of other atoms that are coadsorbed. We use Ho atoms as markers for O and bridge sites to determine the adsorption site of coadsorbed Co adatoms. Figure 8(a) shows a 1-ML-thick MgO region with coadsorbed Ho and Co atoms. The overlaid grid has again been extracted from atomically resolved images of the substrate and then been brought to coincidence with the Ho^A atoms. It therefore marks the O atoms, and one sees that all Co atoms on that image are adsorbed on top of O, in agreement with Ref. [5]. Notice that Co is always on O, independent of the MgO layer thickness (up to three layers), in excellent agreement with DFT. Using
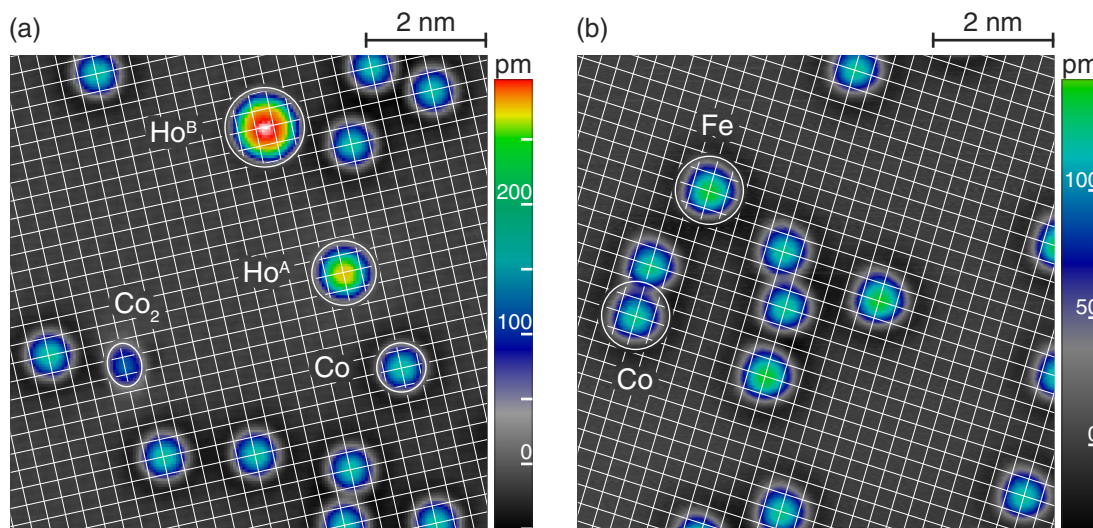

FIG. 8. STM images of (a) coadsorbed Co and Ho and (b) Co and Fe on 1-ML MgO(100)/Ag(100). The lattices are inferred from atomically resolved images of the bare MgO surface of the respective samples and mark the O positions. In (a) $V_t = -20$ mV, $I_t = 20$ pA, and in (b) $V_t = -50$ mV, $I_t = 20$ pA.
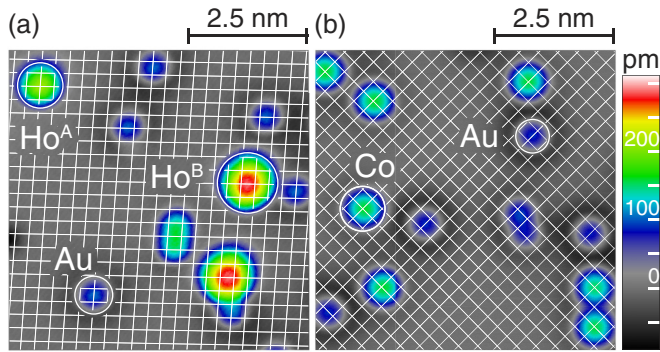
FIG. 9. STM image of coadsorption of (a) Au and Ho and (b) Au and Co on 1-ML MgO/Ag(100). The overlaid lattices mark oxygen positions in both cases. All Au atoms are found on the bridge site. $V_t = -100$ mV and $I_t = 20$ pA in both STM images.

Co as a marker for the O sites, we further determine that Fe also adsorbs on top of O [Fig. 8(b)], confirming previous DFT calculations [3,5,24,53–56]. Additionally, we note the presence of an elongated object with an apparent height of 135 ± 3 pm, marked in Fig. 8. Scanning tunneling spectroscopy reveals inelastic steps at around 10 mV. Therefore, they are identified as Co dimers [57]. We find that their axis is aligned along the O sublattice and each of the two constituent atoms is directly above or at least very close to an O site. This result indicates that our method can be extended to few-atom clusters or small molecules.

E. Adsorption sites of Au on MgO

We now apply our method to Au atoms, for which contradictory results were reported in the literature [29–31]. Figure 9(a) shows 1-ML MgO with coadsorbed Au and Ho and a grid with lattice spacing and orientation again extracted from an atomically resolved bare MgO spot of the same sample. Ho^A and Ho^B atoms are used to align the grid such that it represents the O positions. All the Au atoms shown in Fig. 9(a) are on bridge sites. A statistical analysis over 50 Au atoms on 1-ML MgO indicates that they almost exclusively adsorb on bridge sites, with a small fraction ($8\% \pm 4\%$) found on top of Mg. An equivalent identification done by codepositing Co and Au atoms and using the Co atoms as reference for the O sublattice provides the same result within the error bars [see Fig. 9(b)]. Table I shows that DFT finds the highest binding energy on the bridge site for mono- and bilayer MgO and for the O site on MgO bulk, the latter supporting former EPR experiments [28] and DFT calculations [31].

The use of adsorbates or substitutional atoms as atomic markers is the key to identifying an adatom's adsorption site on ionic or more general multielement surfaces. STM images of Au atoms on 3-ML MgO were interpreted with an atomic lattice that was not calibrated with substitutional doping or other means, and a close to equivalent occupation of O and Mg sites was inferred [29]. A small translation of this lattice by half of its lattice parameter would identify the two species as the two differently oriented bridge sites, thus compatible with our present finding and with former DFT calculations for Au atoms on 1- to 4-ML MgO/Mo(100) [30]. On mono- and bilayer MgO films, the presence of the substrate allows for an effective charge transfer to the adsorbed atom. Conversely, the charge transfer is reduced in the absence of a metal support, as our DFT calculations and Refs. [30,31] show. In addition to the reduced charge transfer to the substrate, DFT predicts a change in the adsorption site from bridge to oxygen going from ultrathin MgO films on Ag(100) to MgO bulk. This result is in agreement with a former EPR experiment, which reported adsorption on top of O for 20-ML MgO/Ag(100) [28]. We therefore infer that the transition between the bridge and the O site occurs for MgO thickness above 3 ML [29].

IV. CONCLUSION

We presented a viable way to experimentally determine the adsorption site of adatoms on surfaces made of two or more elements and to interpret atomically resolved STM images thereof. For the specific case of MgO, we determine the adsorption sites of Ho, Co, Fe, and Au for the MgO mono- and bilayers grown on Ag(100). These results are important for understanding the fascinating electronic, catalytic, and magnetic properties of individual adatoms on thin films of ionic crystals.

ACKNOWLEDGMENTS

[1] A. J. Heinrich, J. A. Gupta, C. P. Lutz, and D. M. Eigler, Science **306**, 466 (2004).

[2] A. F. Otte, M. Ternes, K. v. Bergmann, S. Loth, H. Brune, C. P. Lutz, C. F. Hirjibehedin, and A. J. Heinrich, Nat. Phys. **4**, 847 (2008).

[3] I. G. Rau, S. Baumann, S. Rusponi, F. Donati, S. Stepanow, L. Gragnaniello, J. Dreiser, C. Piamonteze, F. Nolting, S. Gangopadhyay, O. R. Albertini, R. M. Macfarlane, C. P. Lutz, B. A. Jones, P. Gambardella, A. J. Heinrich, and H. Brune, Science **344**, 988 (2014).

[4] S. Baumann, W. Paul, T. Choi, C. P. Lutz, A. Ardavan, and A. J. Heinrich, Science **350**, 417 (2015).

[5] F. Donati, S. Rusponi, S. Stepanow, C. Wäckerlin, A. Singha, L. Persichetti, R. Baltic, K. Diller, F. Patthey, E. Fernandes, J. Dreiser, Ž. Šljivančanin, K. Kummer, C. Nistor, P. Gambardella, and H. Brune, Science **352**, 318 (2016).

[6] W. Paul, K. Yang, S. Baumann, N. Romming, T. Choi, C. P. Lutz, and A. J. Heinrich, Nat. Phys. **13**, 403 (2017).

[7] F. D. Natterer, K. Yang, W. Paul, P. Willke, T. Choi, T. Greber, A. J. Heinrich, and C. P. Lutz, Nature (London) **543**, 226 (2017).

[8] J. Repp, G. Meyer, F. E. Olsson, and M. Persson, Science **305**, 493 (2004).

[9] F. E. Olsson, S. Paavilainen, M. Persson, J. Repp, and G. Meyer, Phys. Rev. Lett. **98**, 176803 (2007).

[10] W. Steurer, J. Repp, L. Gross, I. Scivetti, M. Persson, and G. Meyer, Phys. Rev. Lett. **114**, 036801 (2015).

[11] A. S. Wörz, K. Judai, S. Abbet, J. M. Antonietti, U. Heiz, A. D. Vitto, L. Giordano, and G. Pacchioni, Chem. Phys. Lett. **399**, 266 (2004).

[12] Z. Novotný, G. Argentero, Z. Wang, M. Schmid, U. Diebold, and G. S. Parkinson, Phys. Rev. Lett. **108**, 216103 (2012).

[13] X. F. Yang, A. Wang, B. Qiao, J. Li, J. Liu, and T. Zhang, Acc. Chem. Res. **46**, 1740 (2013).

[14] G. S. Parkinson, Z. Novotny, G. Argentero, M. Schmid, J. Pavelec, R. Kosak, P. Blaha, and U. Diebold, Nat. Mater. **12**, 724 (2013).

[15] R. Bliem, J. van der Hoeven, A. Zavodny, O. Gamba, J. Pavelec, P. E. de Jongh, M. Schmid, U. Diebold, and G. S. Parkinson, Angew. Chem., Int. Ed. **54**, 13999 (2015).

[16] C. Hübner, B. Baxevanis, A. A. Khajetoorians, and D. Pfannkuche, Phys. Rev. B **90**, 155134 (2014).

[17] S. C. Wang and G. Ehrlich, Phys. Rev. Lett. **62**, 2297 (1989).

[18] H. Brune, J. Wintterlin, G. Ertl, and R. J. Behm, Europhys. Lett. **13**, 123 (1990).

[19] J. Repp, G. Meyer, K. H. Rieder, and P. Hyldgaard, Phys. Rev. Lett. **91**, 206102 (2003).

[20] F. Donati, Q. Dubout, G. Autès, F. Patthey, F. Calleja, P. Gambardella, O. V. Yazyev, and H. Brune, Phys. Rev. Lett. **111**, 236801 (2013).

[21] T. Eelbo, M. Waśniowska, M. Gyamfi, S. Forti, U. Starke, and R. Wiesendanger, Phys. Rev. B **87**, 205443 (2013).

[22] N. Lopez and S. Valeri, Phys. Rev. B **70**, 125428 (2004).

[23] A. Malashevich, E. I. Altman, and S. Ismail-Beigi, Phys. Rev. B **90**, 165426 (2014).

[24] H. Y. T. Chen and G. Pacchioni, Phys. Chem. Chem. Phys. **16**, 21838 (2014).

[25] K. Lämmle, T. Trevethan, A. Schwarz, M. Watkins, A. Shluger, and R. Wiesendanger, Nano Lett. **10**, 2965 (2010).

[26] G. Teobaldi, K. Lämmle, T. Trevethan, M. Watkins, A. Schwarz, R. Wiesendanger, and A. L. Shluger, Phys. Rev. Lett. **106**, 216102 (2011).

[27] C. Klein, A. Eichler, E. L. D. Hebenstreit, G. Pauer, R. Koller, A. Winkler, M. Schmid, and P. Varga, Phys. Rev. Lett. **90**, 176101 (2003).

[28] M. Yulikov, M. Sterrer, M. Heyde, H.-P. Rust, T. Risse, H.-J. Freund, G. Pacchioni, and A. Scagnelli, Phys. Rev. Lett. **96**, 146804 (2006).

[29] M. Sterrer, T. Risse, M. Heyde, H.-P. Rust, and H.-J. Freund, Phys. Rev. Lett. **98**, 206103 (2007).

[30] K. Honkala and H. Häkkinen, J. Phys. Chem. C **111**, 4319 (2007).

[31] G. Pacchioni, L. Giordano, and M. Baistrocchi, Phys. Rev. Lett. **94**, 226104 (2005).

[32] J. Pal, M. Smerieri, E. Celasco, L. Savio, L. Vattuone, and M. Rocca, Phys. Rev. Lett. **112**, 126102 (2014).

[33] R. Gaisch, J. Gimzewski, B. Reihl, R. Schlittler, M. Tschudy, and W. Schneider, Ultramicroscopy **42**, 1621 (1992).

[34] P. Blaha, K. Schwarz, G. Madsen, D. Kvasnicka, and J. Luitz, WIEN2k: An Augmented Plane Wave plus Local Orbitals Program for Calculating Crystal Properties (Karlheinz Schwarz, Techn. Universität Wien, Austria, 2001).

[35] J. Enkovaara, C. Rostgaard, J. J. Mortensen, J. Chen, M. Dułak, L. Ferrighi, J. Gavnholt, C. Glinsvad, V. Haikola, H. A. Hansen, H. H. Kristoffersen, M. Kuisma, A. H. Larsen, L. Lehtovaara, M. Ljungberg, O. Lopez-Acevedo, P. G. Moses, J. Ojanen, T. Olsen, V. Petzold, N. A. Romero, J. Stausholm-Møller, M. Strange, G. A. Tritsaris, M. Vanin, M. Walter, B. Hammer, H. Häkkinen, G. K. H. Madsen, R. M. Nieminen, J. K. Nørskov, M. Puska, T. T. Rantala, J. Schiøtz, K. S. Thygesen, and K. W. Jacobsen, J. Phys. Condens. Matter **22**, 253202 (2010).

[36] P. E. Blöchl, Phys. Rev. B **50**, 17953 (1994).

[37] J. J. Mortensen, L. B. Hansen, and K. W. Jacobsen, Phys. Rev. B **71**, 035109 (2005).

[38] J. P. Perdew, K. Burke, and M. Ernzerhof, Phys. Rev. Lett. **77**, 3865 (1996).

[39] V. I. Anisimov, J. Zaanen, and O. K. Andersen, Phys. Rev. B **44**, 943 (1991).

[40] S. L. Dudarev, G. A. Botton, S. Y. Savrasov, C. J. Humphreys, and A. P. Sutton, Phys. Rev. B **57**, 1505 (1998).

[41] H. J. Monkhorst and J. D. Pack, Phys. Rev. B **13**, 5188 (1976).

[42] D. C. Liu and J. Nocedal, Math. Program. **45**, 503 (1989).

[43] S. Baumann, I. G. Rau, S. Loth, C. P. Lutz, and A. J. Heinrich, ACS Nano **8**, 1739 (2014).

[44] S. Schintke, S. Messerli, M. Pivetta, F. Patthey, L. Libioulle, M. Stengel, A. De Vita, and W.-D. Schneider, Phys. Rev. Lett. **87**, 276801 (2001).

[45] J. Wollschläger, J. Viernow, C. Tegenkamp, D. Erdös, K. M. Schröder, and H. Pfnür, Appl. Surf. Sci. **142**, 129 (1999).

[46] S. Valeri, S. Altieri, A. d. Bona, P. Luches, C. Giovanardi, and T. S. Moia, Surf. Sci. **507**, 311 (2002).

[47] S. Stankic, M. Sterrer, P. Hofmann, J. Bernardi, O. Diwald, and E. Knözinger, Nano Lett. **5**, 1889 (2005).

[48] P. W. Tasker, E. Colbourn, and W. MacKrodt, J. Am. Ceram. Soc. **68**, 74 (1985).

[49] R. C. McCune and P. Wynblatt, J. Am. Ceram. Soc. **66**, 111 (1983).

[50] D. Z. Gao, M. B. Watkins, and A. L. Shluger, J. Phys. Chem. C **116**, 14471 (2012).

[51] O. Bünermann, H. Jiang, Y. Dorenkamp, A. Kandratsenka, S. Janke, D. J. Auerbach, and A. M. Wodtke, Science **350**, 1346 (2015).

[52] H. Brune, Science **350**, 1321 (2015).

[53] A. Markovits, J. C. Paniagua, N. López, C. Minot, and F. Illas, Phys. Rev. B **67**, 115417 (2003).

[54] K. Neyman, C. Inntam, V. Nasluzov, R. Kosarev, and N. Rösch, Appl. Phys. A **78**, 823 (2004).

[55] S. Baumann, F. Donati, S. Stepanow, S. Rusponi, W. Paul, S. Gangopadhyay, I. G. Rau, G. E. Pacchioni, L. Gragnaniello, M. Pivetta, J. Dreiser, C. Piamonteze, C. P. Lutz, R. M. Macfarlane, B. A. Jones, P. Gambardella, A. J. Heinrich, and H. Brune, Phys. Rev. Lett. **115**, 237202 (2015).

[56] O. R. Albertini, A. Y. Liu, and B. A. Jones, Phys. Rev. B **91**, 214423 (2015).

[57] S. Baumann, Ph.D. thesis, University of Basel, 2015.